Mechatronic Systems and Control, Vol. 50, No. 10, 2022
An Open Access Paper

IMPROVED COMPRESSED SENSING RECONSTRUCTION FOR FLUORESCENCE MOLECULAR TOMOGRAPHY OF SPARSE VIEW

Zhaolu Zuo,* Shaobin Dou,* and Deyi Kong,*,**

Abstract

With the development of fluorescence molecular tomography technology, densely sampled measurements can be easily obtained. However, challenges still remain in fast image reconstruction, phototoxicity, photobleaching of the fluorescent proteins, long time under anesthetic and specimen movement during the acquisition, etc. In this work, a novel compressed sensing reconstruction method was presented to reduce the acquisition time or number of projections, while yielding better image quality. We defined a differentiable convex total variation function as the optimization objective, which improved the calculation speed and stability of the finite difference transform. In addition, maximum likelihood expectation maximization algorithm was proposed as the projection onto convex sets process to improve the convergence speed of the algorithm. For testing and evaluating the proposed algorithm, we also designed a head model of emission mode in MATLAB. Phantom simulations demonstrated that the proposed method could achieve fine reconstruction image by sparse view.

Key Words

Fluorescence molecular, compressed sensing, image reconstruction, sparse view

1. Introduction

In vivo, with the help of fluorescent probes, fluorescence signals can express molecular and cellular activities. Fluorescence molecular tomography (FMT) can be applied to study many physiological and pathological processes in small animal. In principle, it is an optical version of the single photon emission computed tomography without collimator. A large number of research works has shown such benefits that the method could provide. Compared with other imaging techniques, FMT has superiorities of sensitivity and specificity. Fluorescence is generated under external laser excitation or during metabolism. To obtain the three-dimensional distribution of fluorescence in the tissue, multi-angle detection of fluorescent photons escaping from the body surface, through three-dimensional reconstruction. FMT can realize the physiological and biochemical process of tissues, the pharmacokinetic process of targeted drugs, etc., *in vivo*, continuous, and noninvasive observation [1]. It has become an important tool for biomedical research, diseases diagnosis, therapies evaluation, and so on [2]. For FMT, it is important to reduce the light dose and the acquisition time [3]. The excessive amount of light dose may cause photo-toxicity of the fluorescent proteins, and the excessive acquisition time may lead to the undesirable movement of samples. In addition to speeding up the scan speed, an effective way is to reduce the number of the projection. With filtered back projection (FBP), the number of projections necessary to reconstruct accurately should be proportional to the resolution of the projection image [4]. In the case of sparse angle, the result of FBP reconstruction has strip artifacts, and the image details are completely blurred [5]–[7]. The compressed sensing (CS), also known as compressive sensing, compressive sampling, or sparse sampling algorithm, is a new technique for acquiring and reconstructing a signal [8], [9]. Random sampling is used to obtain discrete samples of the signal, and then the signal is perfectly reconstructed through a nonlinear reconstruction algorithm. The theory of CS indicates that a signal can be recovered from far fewer samples than required by the Shannon–Nyquist sampling theorem by exploiting the sparsity of it [10]. But CS is limited by two basic conditions. The first is sparsity, which requires the signal is sparse in some domain; and the second one is incoherence between the measurement matrix and the sparse basis. Most medical images do not satisfy the requirement of sparsity. But most of them can get sparse representation by sparse transformation. So the CS-based algorithm may be used to reconstruct images from sparse projection data

* Hefei Institutes of Physical Science, Chinese Academy of Sciences, 230031, Hefei, China; e-mail: zuozl@iim.ac.cn, 337471801@qq.com
** Innovation Academy for Seed Design, Institute of Genetics and Developmental Biology, CAS, 100101, Beijing, China; e-mail: kongdy@iim.ac.cn
Corresponding author: Shaobin Dou
Recommended by Dr. Min Xia
(DOI: 10.2316/J.2022.201-0288)

[11]–[14]. Most of these iterative processes of CS algorithm are based on an implementation of the algebraic reconstruction technique (ART) or expectation maximization transform that acts as forward projector [15]. In the ART algorithm, the factors that affect the number of iterations and the quality of reconstruction mainly include the access mode of projection data and the selection of relaxation factors. These two parameters are often related to the number of projections and the features of the image, which are difficult to determine usually. In this paper, we present a novel CS algorithm using maximum likelihood expectation maximization (MLEM) algorithm [16] as the projections onto convex sets (POCS) process [17], [18] to avoid such problems. The simulation experiment and reconstruction effect evaluation were also carried out.

The paper was organized as follows. In Section 2, the basic concepts of CS related to this article will be introduced briefly. In Section 3, the proposed improved compression sensing algorithm will be discussed in detail, and in Section 4, the reconstructed and original image at the visualization-based evaluation levels and quantitative-metric-based comparison levels are carried out. Finally, the implication of the results will be further discussed in Section 5.

2. Preliminaries

2.1 The Sparsity and Sparse Representation

The sparsity of a signal is that the signal can be represented by a linear combination of a few feature vectors. Let $X = [x_1, x_2, \ldots, x_n]^T$, $X \in R^N$, represent a one-dimensional discrete signal with length N, and X can be represented by a linear combination of a set of orthogonal bases $D = [d_1, d_2, \ldots, d_N]$, $N \in R^N$,

$$x = \sum_{i=1}^{N} \Psi_i s_i = \Psi s \tag{1}$$

there are only K nonzero coefficients in S. The commonly used sparse bases include discrete cosine transform basis, discrete wavelet transform basis, fast Fourier transform basis, chirplet basis, and curvelet basis. Normally, these transformations can obtain good sparse representation, but the computation process is rather complicated.

2.2 Sparse Sampling

After the sparse representation of the signal is obtained by sparse transformation, the observation value y of length $M(M \ll N)$ can be acquired:

$$y = \Phi x = \Phi\Psi s = \Theta s, \quad \Theta = \Phi\Psi \tag{2}$$

where Φ is the observation matrix ($M \times N$), and Ψ is the sparse basis. It is an underdetermined problem to recover the N-dimensional vector x from the M-dimensional vector y, when $M \ll N$. The sufficient and necessary condition for the solvability of the problem is that for given $\varepsilon > 0$, the vector v with K nonzero terms and the measurement matrix Θ satisfy the following restricted isometry property (RIP) conditions (Candes and Tao):

$$1 - \varepsilon \leq \frac{\|\Theta v\|_2}{\|v\|_2} \leq 1 + \varepsilon \tag{3}$$

2.3 Recovery

When the matrix Θ satisfies the RIP characteristic, the sparse coefficient s can be obtained by inversing (2), and then the signal x can be accurately recovered from the M-dimensional observation vector through (1). The reconstruction of signals is essentially a process of finding the sparsest solution under the condition that y can be obtained, that is, the problem of solving the underdetermined equations. The most direct method to solve the problem is by minimizing the l_0 norm:

$$\min_s \|s\|_0 \, s.t. y = \Phi\Psi s \quad \text{or} \quad \min_s \|s\|_0 \, s.t. \, \|\Phi\Psi s - \mathrm{y}\|_2^2 \leq \varepsilon \tag{4}$$

where $\|s\|_0$ denotes the number of nonzero elements of s. The l_0 norm constraint objective function is a NP-hard problem. It has been proved that l_0 norm minimization and l_1 norm minimization are equivalent under certain conditions (Terry tao). The problem can be transformed into the l_1 norm minimization problem:

$$\min_s \|s\|_1 \, s.t. y = \Phi\Psi s \quad \text{or} \quad \min_s \|s\|_1 \, s.t. \, \|\Phi\Psi s - \mathrm{y}\|_2^2 \leq \varepsilon, \; \|s\|_1 = \sum_{i=1}^{n} s_i \tag{5}$$

It's a convex optimization problem, which can be solved by linear programming. The typical algorithms include gradient projection method, interior point method, basis pursuit, and POCS algorithm. In addition, some greedy algorithms can be used to solve such problem.

3. Proposed Method

Due to the characteristics of biological tissue and FMT imaging, the fluorescence image has characteristic of local smoothing, and it can be considered that its finite difference image is sparse. Our experiments show that the finite difference image of FMT has good sparsity and can reflect the edge information of the image. So, the finite difference transform (FDT) is used as its sparse transformation. The l_1 norm of the FDT, that is, the total variation (TV), is taken as the optimization objective function. The TV is defined as:

$$\begin{aligned} \mathrm{TV}(F) &= \int_\Omega \sqrt{|\nabla F|^2} dxdy \\ &= \int_\Omega \sqrt{|\partial F/\partial x|^2 + |\partial F/\partial y|^2} dxdy \end{aligned} \tag{6}$$

The function is homogeneous, but not differentiable and not convex. The speed and stability of solving non-convex

functions are worse than convex functions. Here, we define two-dimensional TV as another form:

$$\begin{aligned}\mathrm{TV}(F) &= \int_{\Omega}\sqrt{|\nabla F|^2}dxdy \\ &= \int_{\Omega}\sqrt{|\partial F/\partial x|^2}dxdy + \int_{\Omega}\sqrt{|\partial F/\partial \mathrm{y}|^2}dxdy \end{aligned} \quad (7)$$

For two-dimensional image, the FDT can be defined as:

$$TV\left(F\right) = \sum_{i,j}\left(\sqrt{\left(f_{i,j}-f_{i-1,j}\right)^2} + \sqrt{\left(f_{i,j}-f_{i,j-1}\right)^2}\right) \quad (8)$$

Then, the image F can be reconstructed by solving the following optimization problems:

$$\min TV\left(F\right), s.t. P = AF, F \geq 0 \quad (9)$$

where P is the fluorescence projection image, A is the observation matrix, and F is the image to be reconstructed. The constraint condition $P = AF$ is implemented by POCS algorithm. The optimization problem is solved by gradient descent method.

For the scanning mode of fluorescence molecular image, the measurement matrix is approximate to an irregular local Fourier transform operator, which satisfies the RIP characteristic. So, the reconstruction problem from the sparse sampling signal has a stable solution.

The concrete implementation process consists of two steps, one is the MLEM process under the constraint condition and the other is the process of solving the total variation minimization (TVM).

The fluorescence image reconstruction process of POCS-TVM is as follows:

Step 1, POCS process

(1) Initialize reconstruction image:

$$F^0_{\mathrm{MLEM}}\left(k=0\right) = 0 \quad (10)$$

where k is the total number of iterations.

(2) Iterate over the image using MLEM algorithm:

$$f_j^{(k+1)} = f_j^{(k)}\frac{1}{\sum_i a_{i,j}}\sum_i a_{i,j}\frac{p_i}{\sum_l a_{i,l}f_l^{(k)}} \quad (11)$$

here, k is the total number of iterations, $f_j^k$is the estimated value after k iterations, $p_i$is the i-th projection value, and $a_{i,j}$represents the probability that the photon emitted from the pixel $j$of the object is detected by the detector unit i.

(3) Nonnegative constraint on calculated value:

$$F_{MLEM}\left(k\right) = \begin{cases} F^M_{MLEM}\left(k\right), & F^M_{MLEM}\left(k\right) \geq 0 \\ 0, & F^M_{MLEM}\left(k\right) < 0 \end{cases} \quad (12)$$

Step 2, TVM process

(1) Initialize the TVM image:

$$F^0_{TVM}\left(k\right) = F_{POCS}\left(k\right) \quad (13)$$

(2) Calculate the increment factor:

$$d\left(k\right) = \left\|X^0_{MLEM}\left(k\right)X_{POCS}\left(k\right)\right\| \quad (14)$$

(3) Calculate the gradient of TV and its direction:

$$\begin{aligned}\vec{G}^{n-1}\left(k\right) &= \left.\frac{\partial\left\|F\right\|_{TV}}{\partial f_{i,j}}\right|_{F=F^{n-1}_{TVM}(k)}, \\ \hat{G}^{n-1}\left(k\right)&\frac{\vec{G}^{n-1}\left(k\right)}{\left|\vec{G}^{n-1}\left(k\right)\right|}\end{aligned} \quad (15)$$

where n is the ordinal number of TVM processes.

(4) Modify the image in the negative direction of the gradient:

$$F^m_{TVM}\left(k\right) = F^{m-1}_{TVM}\left(k\right) - \lambda d_A\left(k\right)\hat{G}^{n-1}\left(k\right),\ n = n+1 \quad (16)$$

where λ is a regulator. If the result of the calculation satisfies the conditions:

$$\left\|F^k_{POCS}\left(k\right) < F^{K-1}_{POCS}\left(k\right)\right\| < \varepsilon \quad (17)$$

the algorithm terminates.

Otherwise:

$$F^0_{MLEM}\left(k+1\right) = F^N_{TVM}\left(k\right) \quad (18)$$

A new iterative process was carried out.

4. Experiment and Evaluation

4.1 Subjective Index

In order to demonstrate the effectiveness of the proposed algorithm, we designed a Shepp–Logan head model of emission mode as experimental phantom in MATLAB. The model is often used to verify the effect of image reconstruction. The photons are radiated from the inside of the model and attenuated by the tissue on the transmission path [19], [20]. In the range of 360 degrees, a detector is used to receive photons and obtain projection images. Then, the projection images are reconstructed using FBP and the improved CS algorithm proposed, respectively.

FBP algorithm is often used in 3D image reconstruction algorithm, due to its fast reconstruction time [21], [22]. When sufficient projection images are provided, the FBP algorithm can produce high-quality reconstruction images, which is often used as the criterion of other reconstruction algorithms. Using 360, 180, 90, 60, 30, and 18 projections, POCS-TVM and FBP algorithms are used for reconstruction, respectively. Figure 1 shows the comparisons. The first row is the FBP reconstruction image, and the second is that of POCS-TVM. Intuitively, we can see that the image quality of FBP algorithm is equal to that of POCS-TVM when the number of projections is more than 180. When the number of projections is less than 90, the image of FBP has obvious artifacts, while POCS-TVM has better performance. It's difficult to reconcile the demands of image quality and artifact elimination when the number of projections is less than 30.

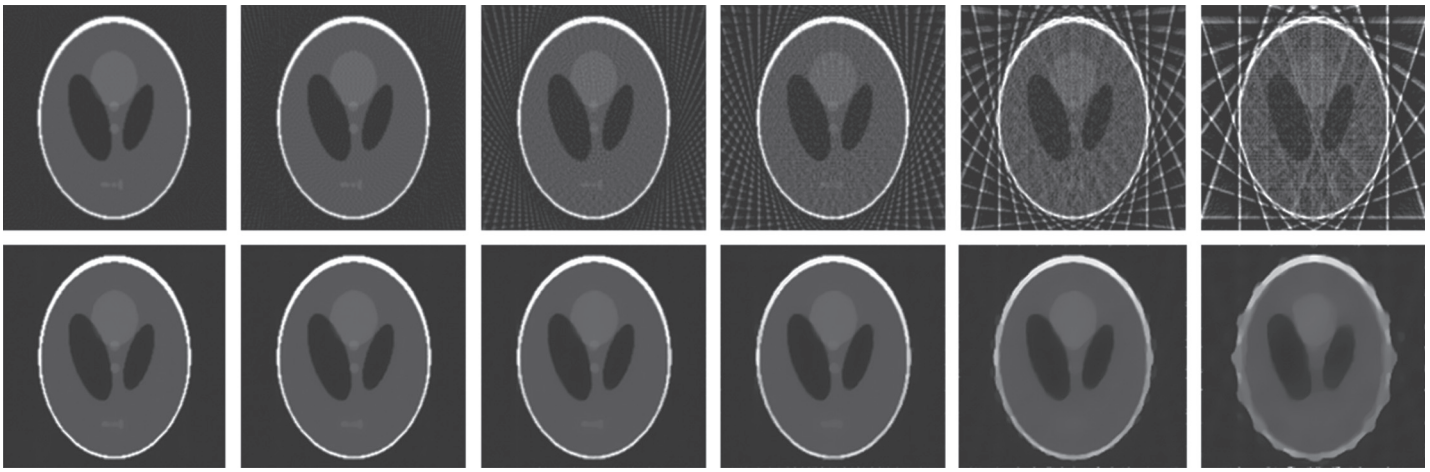

Figure 1. The comparison of reconstructed image between POCS-TVM and FBP. In sequence, (a) to (e) belongs to 360 to 30 projections, respectively.

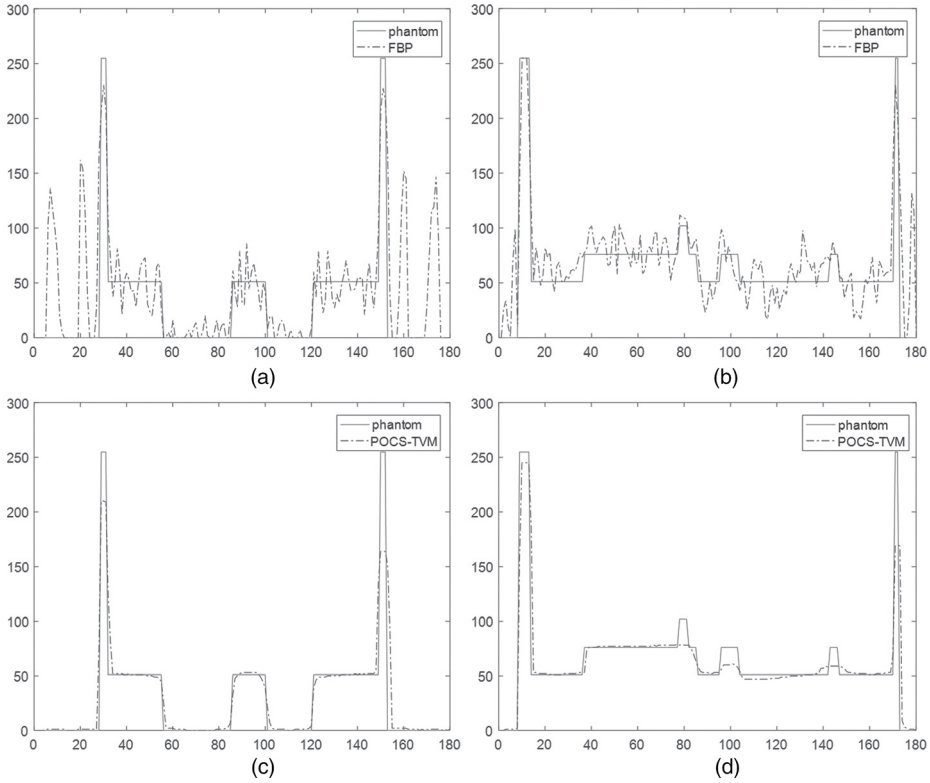

Figure 2. (a) and (b) is horizontal and vertical center profile line of FBP image, respectively, (c) and (d) belongs to that of POCS-TVM.

4.2 Objective Index

Since it is difficult to obtain better quality of reconstruction image quality, 30 projections are used in the following experiments. In order to accurately compare the difference between the reconstructed image and the original image, we take the longitudinal and horizontal central profile lines as the comparison object, respectively (Fig. 2). It can be clearly seen that the reconstructed image by POCS-TVM algorithm is very close to the original image, while that of FBP is very different, and has obvious artifact noise.

The mean squared error (MSE) is the mathematical expectation of the squared error between the two values. For two-dimensional image:

$$MSE = \frac{1}{m.n} \sum_{i=0}^{m-1} \sum_{j=0}^{n-1} \left\| I(i,j) - \hat{I}(i,j) \right\|^2 \qquad (19)$$

Table 1
Image Quality Comparison and Evaluation between FBP and POCS-TVM Reconstruction

Style Name	RMSE	PSNR	SSIM
POCS-TVM	3.49	20.98	0.85
FBP	9.15	16.00	0.27

Its square root, root mean square error (RMSE) can be used to measure the deviation between the reconstructed image and the original image:

$$RMSE = \sqrt{MSE} = \sqrt{\frac{1}{m.n}\sum_{i=0}^{m-1}\sum_{j=0}^{n-1}\left\|I(i,j) - \hat{I}(i,j)\right\|^2} \tag{20}$$

Here, $I(i,j)$and $\hat{I}(i,j)$ are original image and reconstructed image pixel, respectively. A smaller RMSE value indicates a smaller difference.

The peak signal-to-noise ratio (PSNR) is an error-sensitive image quality evaluation. The larger the PNSR value, the smaller the distortion of reconstructed image:

$$PSNR = 10 \times \log_{10}\left(\frac{MAX_I^2}{MSE}\right) = 20 \times \log_{10}\left(\frac{MAX_I}{MSE}\right) \tag{21}$$

Here, MAX_I is the maximum value of the image.

The structural similarity (SSIM) is an index to measure the similarity of two digital images:

$$SSIM\,(X,G) = \frac{(2\mu_X\mu_G + c_1)(2\sigma_{XG} + c_2)}{(\mu_X^2 + \mu_G^2 + c_1)(\sigma_X^2 + \sigma_G^2 + c_2)} \tag{22}$$

where X and G are the reconstructed image and original image, respectively. The μ_X and μ_G are the average of X and G, σ_X and σ_G are the standard deviations of X and G, and σ_{XG} is the covariance. $C_1 = (K_1 \times L)^2$, $K_1 = 0.01$, and $C_2 = (K_2 \times L)^2$, $K_2 = 0.03$ is a constant used to maintain stability. L is the dynamic range of the image.

From Table 1, we can see that the improved POCS-TVM algorithm can achieve better reconstruction results under 30 sparse projection angles.

5. Conclusion

In this study, an improved CS reconstruction algorithm based on POCS-TVM for FMT has been presented, and the reconstruction process was discussed in detail and verified by experiments. A sort of head model of the emission mode was designed in MATLAB as the test phantom. By using the phantom, the proposed algorithm was tested. Through subjective perception and objective evaluation, we demonstrated that the improved CS algorithm can yield superior performance from sparse view projection. Experiments showed that, by using as few as 30 sparse view projections, the improved CS reconstruction algorithm could produce high-quality FMT image.

Acknowledgment

This research has been funded by the Key Project of the Chinese Academy of Sciences (KFZD-SW-309) and the General Program of National Natural Science Foundation of China (61573334, 31571567).

References

[1] S. Florian, R. Jorge, and R. Markus, Fluorescence molecular tomography: principles and potential for pharmaceutical research, *Pharmaceutics, 3*(2), 2011, 229–274.

[2] A. Farina, *et al.*, Multiple-view diffuse optical tomography system based on time-domain compressive measurements, *Optic Letters, 42*(14), 2017, 2822–2825.

[3] M. Toms, *et al.*, Spectral domain optical coherence tomography: An in vivo imaging protocol for assessing retinal morphology in adult Zebrafish, *Zebrafish 14*(2), 2017, 118–125.

[4] T. Correia, *et al.*, Accelerated optical projection tomography applied to in vivo imaging of Zebrafish, *Plos One, 10*(8), 2015, e0136213.

[5] A.K. Trull, *et al.*, Comparison of image reconstruction techniques for optical projection tomography, *Applied Optics, 57*(8), 2018, 1874–1882.

[6] J.R. Walls, *et al.*, Correction of artefacts in optical projection tomography, *Physics in Medicine & Biology, 50*(19), 2005, 4645–4665.

[7] J.R. Walls, *et al.*, Resolution improvement in emission optical projection tomography, *Physics in Medicine & Biology,* 52(10), 2007, 2775–2790.

[8] E.J. Cands, *et al.*, Robust uncertainty principles: exact signal reconstruction from highly incomplete frequency information, *IEEE Transactions on Information Theory, 52*(2), 2006, 489–509.

[9] D.L. Donoho, Compressed sensing, *IEEE Transactions on Information Theory, 52*(4), 2006, 1289–1306.

[10] E.J. Candes and M.B. Wakin, An introduction to compressive sampling, *IEEE Signal Processing Magazine, 25*(2), 2008, 21–30.

[11] Q. Pi, R. Yao, *et al.*, Wide-field fluorescence molecular tomography with compressive sensing based preconditioning, *Biomedical Optics Express, 6*(12), 2015, 4887–4898.

[12] W. Zou and X. Pan, Compressed-sensing-based fluorescence molecular tomographic image reconstruction with grouped sources, *BioMedical Engineering on Line, 13*(1), 2014, 1–15.

[13] J.F.P.J. Abascal *et al.*, A novel prior- and motion-based compressed sensing method for small-animal respiratory gated CT, *Plos One, 11*(3), 2016, e0149841.

[14] H. Lee *et al.*, Improved compressed sensing-based cone-beam CT reconstruction using adaptive prior image constraints, *Physics in Medicine & Biology, 57*(8), 2012, 2287–2307.

[15] J. Chen *et al.*, A hybrid architecture for compressive sensing 3-D CT reconstruction, *IEEE Journal on Emerging & Selected Topics in Circuits & Systems, 2*(3), 2012, 616–625.

[16] H.Z. Wieczorek, The image quality of FBP and MLEM reconstruction, *Journal of Physics in Medicine & Biology, 55*(11), 2010, 3161.

[17] T. Gomi and Y. Koibuchi, Use of a total variation minimization iterative reconstruction algorithm to evaluate reduced projections during digital breast tomosynthesis, *Biomed Research International*, 2018, 1–14. doi: 10.1155/2018/5239082.

[18] X. Lv, X. Wang, Z. Tian, *et al.*, Design of automatic reseeding system of air suction precision metering seeding device for corn, *Mechatronic Systems and Control, 48*(3), 2020, doi:10.2316/J.2020.201-0038

[19] J. Dey and M.A. King, Theoretical and numerical study of MLEM and OSEM reconstruction algorithms for motion correction in emission tomography, *IEEE Transactions on Nuclear Science, 56*(5), 2009, 2739–2749.

[20] F. Arcadu, *et al.*, A forward regridding method with minimal oversampling for accurate and efficient iterative tomographic algorithms, *IEEE Transactions on Image Processing, 25*(3), 2016, 1207–1218.

[21] J. Cai, P. Gao, Y. Wu, *et al.*, Mobile robot navigation using monocular visualinertial fusion, *Mechatronic Systems and Control, 49(1)*, 2021, doi:10.2316/J.2021.201-0100.

[22] J. Zou and H. Zhang, New key point detection technology under real-time eye tracking, *Mechatronic Systems and Control*, *47*(2), 2019. doi:10.2316/J2019.201-2969.

Biographies

Zhaolu Zuo was born in Jinlin, China in 1984. He received the Ph.D. degree in optics from University of Science and Technology of China, Hefei, China, in 2020. He is currently a postdoctoral in Hefei Institutes of Physical Science, Chinese Academy of Sciences. He is the author of more than 10 papers and more than 20 inventions. His research interests include machine vision and fluorescence tomography (FMT) reconstruction algorithm research.

Shaobin Dou was born Anhui, China in 1979. He received the Ph.D. degree in optics from University of Science and Technology of China, Hefei, China, in 2019. He has long been engaged in the research of medical image processing and reconstruction algorithms, as well as the research and development of software and hardware, mainly including X-ray CT reconstruction algorithm research, positron emission tomography (PET) reconstruction algorithm research, fluorescence tomography (FMT) reconstruction algorithm research.

Deyi Kong was born in Anhui, China in 1966. He received the B.S degree in physics from Hefei University of Technology in 1990, the M.S. degree in physics from University of Science and Technology of China in 1993, and the Ph.D degree in microelectronics from Southeast University in 1999. From 2000 to 2004, he was an Associate Professor in the Institute of Intelligent Machines, Chinese Academy of Sciences. Since 2005, he has been a Professor in the Hefei Institutes of Physical Science, Chinese Academy of Sciences. He is the author of more than 100 papers and more than 60 inventions. His research interests include microsensors, microsystems, and biomimetic robots.